Acta Crystallographica Section D
Biological Crystallography
ISSN 0907-4449

A structural double-mutant cycle: estimating the strength of a buried salt bridge in barnase

Cara K. Vaughan,[a] Pia Harryson,[b]† Ashley M. Buckle[c] and Alan R. Fersht[c]*

[a]Section of Structural Biology, The Institute of Cancer Research, Chester Beatty Laboratories, 237 Fulham Road, London SW3 6JB, England, [b]Department of Plant Physiology, Umea University, S-901 87 Umea, Sweden, and [c]MRC Centre for Protein Engineering, Hills Road, Cambridge CB2 2QH, England

† Present address: Lund University, PO Box 124, S-22100 Lund, Sweden.

Correspondence e-mail: arf25@cam.ac.uk

Received 16 October 2001
Accepted 24 January 2002

PDB References: RS69 mutant, 1b20; RS69:DN93 mutant, 1b21; DN93 mutant, 1b2z; wild type, 1b2x.

Double-mutant cycles are widely used in the field of protein engineering to measure intermolecular and intramolecular interactions. Ideally, there should be no structural rearrangement of the protein on making the two single mutations and the double mutation within the cycle. However, structural pertubation on mutation does not preclude the use of this method, providing the sum of the changes in the single mutants equals the change in the double mutant. In this way, the energy associated with any structural rearrangement cancels in the double-mutant cycle. Previously, the contribution of a buried salt bridge between Arg69 and Asp93 in barnase to the stability of the folded protein has been determined by double-mutant cycle analysis. In order to determine whether the measured interaction of -14.0 kJ mol^{-1} represents the true interaction energy, the crystal structure of each mutant within the double-mutant cycle was solved. Although mutation results in structural shifts, the majority of those in the single mutants are also found in the double mutant; their energetic effects in the double-mutant cycle are therefore cancelled. This study highlights the robust nature of the double-mutant cycle analysis.

1. Introduction

The experimentally determined contribution of salt bridges to the stability of proteins is highly context dependent. Engineered and wild-type salt bridges on the surface of barnase, T4 lysosyme and CI-2 (Dao-Pin *et al.*, 1991; de Prat Gay *et al.*, 1994; Horovitz *et al.*, 1990; Sali *et al.*, 1991; Serrano *et al.*, 1990) contribute between 0.4 and 2.1 kJ mol^{-1} to the overall stability of the protein. Formation of networks of salt bridges, however, can increase the contribution of each individual salt bridge to the stability of the protein by energetic coupling of the structurally linked salt bridges (Horovitz *et al.*, 1990; Marqusee & Sauer, 1994). Buried salt bridges in chymotrypsin and T4 lysosyme have been observed to contribute between 12.5 and 20.1 kJ mol^{-1} to stability relative to a state in which one partner is mutated leaving a charged unpaired residue (Anderson *et al.*, 1990; Fersht, 1972). Several recent studies have shown that buried salt bridges are destabilizing relative to their hydrophobic counterparts owing to the large and unfavourable energy required to desolvate charges (Hendsch & Tidor, 1994; Waldburger *et al.*, 1995; Wimley *et al.*, 1996).

The role of salt bridges in determining the rate and pathway of folding and unfolding has been investigated for several proteins (Cavagnero *et al.*, 1998; Waldburger *et al.*, 1995, 1996). Salt bridges have also been shown to be important for the specificity of a fold. This has been demonstated conclusively for α-helical coiled coils in both designed *de novo* peptides and

basic leucine zippers from transcription factors such as GCN4, the Fos and Jun proteins and members of the C/EBP and ATF/CREB families (Monera *et al.*, 1994; O'Shea *et al.*, 1992; Schneider *et al.*, 1997; Vinson *et al.*, 1993; Zhou *et al.*, 1994*b*).

Tissot *et al.* (1996) have determined the contribution of a buried salt bridge to the stability and folding of barnase, a small extracellular endonuclease from *Bacillus amyloliquefaciens* (M_r = 12 382). This salt bridge is between Arg69, in $loop_3$ and Asp93 in β-$turn_{3-4}$ linking the third and fourth β-strands (Fig. 1). Using a φ-value analysis (Fersht *et al.*, 1992; Horovitz, 1992) the salt bridge was determined to be almost fully formed in the transition state of the folding pathway. This interaction is therefore formed early in the folding process. These results were confirmed in a study examining the effect of pH on the folding rate of the mutant Asp93→Asn compared with the wild type (Oliveberg & Fersht, 1996). Further, this study showed that disrupting the Arg69–Asp93 salt bridge in this way alters the folding pathway of the protein. The strength of the salt bridge in the fully folded protein was also measured using double-mutant cycle analysis and calculated to be worth 14.0 kJ mol^{-1} (Table 1).

Double-mutant cycles can be used to determine the interaction of two residues *X* and *Y* in a folded protein *E-XY* relative to their interaction in the unfolded state (Carter *et al.*, 1984; Horovitz, 1987; Horovitz & Fersht, 1990; Serrano *et al.*, 1990). The interaction energy $\Delta\Delta G_{\rm int}$ is defined as

$$\Delta\Delta G_{\rm int} = \Delta\Delta G_{E\text{-}XY\rightarrow E\text{-}X} - \Delta\Delta G_{E\text{-}Y\rightarrow E}, \qquad (1)$$

where $\Delta\Delta G_{E\text{-}XY\rightarrow E\text{-}X}$ is the difference in the free energy of unfolding of the wild-type protein *E-XY* and the single mutant *E-X* in which *Y* has been mutated; $\Delta\Delta G_{E\text{-}Y\rightarrow E}$ is the difference in the free energy of unfolding of the single mutant *E-Y* in which *X* has been mutated and *E*, the double mutant in which both *X* and *Y* are mutated. A thermodynamic cycle is set up between the wild type, each of the single mutants and the double mutant. The difference in the energy of parallel sides of the cycle is $\Delta\Delta G_{\rm int}$. $\Delta\Delta G_{\rm int}$ is an estimate of the interaction between the two residues involved in the ideal situation where there is no structural rearrangement on mutating *X* and *Y* or if the energies associated with any resulting structural changes cancel in the thermodynamic cycle. This has been described in detail previously (Fersht *et al.*, 1992; Serrano *et al.*, 1990).

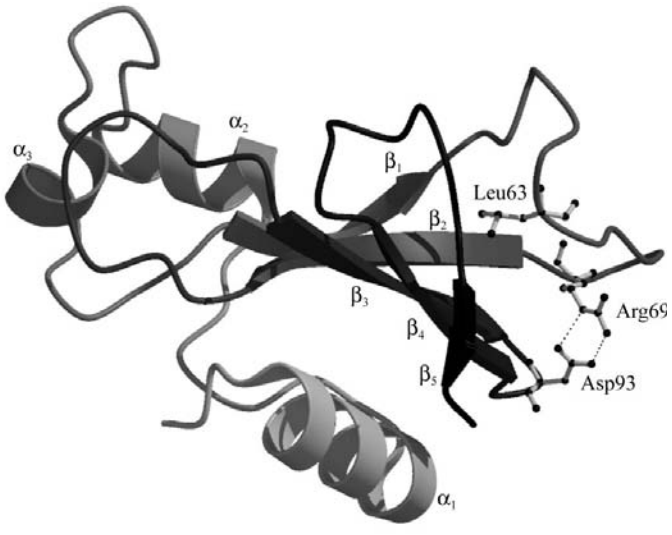

Figure 1
A ribbon diagram of barnase, colour coded from white to black according to sequence. The residues Arg69 and Asp93, which form a buried salt bridge, are drawn in ball-and-stick representation. Leu63, which anchors the centre of $loop_3$ in hydrophobic $core_3$ is also drawn. Drawn with *BOBSCRIPT* (Esnouf, 1997; Kraulis, 1991) and rendered using *Raster3D* (Merritt & Bacon, 1997).

Table 1
Stability of the salt-bridge mutants relative to wild type and the salt-bridge interaction energy.

All data from Tissot *et al.* (1996).

Protein	$\Delta\Delta G_{D\text{-}F}$† (kJ mol^{-1})	$\Delta\Delta G_{F,\ \rm int}$‡ (kJ mol^{-1})	Activity relative to wild type (%)
RS69	11.4	—	86
DN93	17.2	—	92
RS69:DN93	14.6	14.0	67

† The difference in the free energy of unfolding of the mutant and wild type, $\Delta\Delta G_{D\text{-}F} = (\Delta G^{\rm wt} - \Delta G^{\rm mut})_{D\text{-}F}$. ‡ The interaction energy measured by double-mutant cycle analysis. See text.

In order to determine whether the interaction energy measured by Tissot *et al.* (1996) for the buried salt bridge between Arg69 and Asp93 in barnase is a true estimate of the strength of the interaction, we have crystallized and solved the structure of the wild type and each mutant in the double-mutant cycle by X-ray diffraction. These are Arg69→Ser (mutant RS69), Asp93→Asn (mutant DN93) and the double mutant combining the two (mutant RS69:DN93). The extent of destabilization of these mutants relative to the wild type is listed in Table 1.

We show that in the case of this buried salt bridge the majority of the new interactions made in the single mutants are also made in the double mutant. The energetic terms associated with these changes cancel in the double-mutant cycle. The estimate of the interaction energy for this salt bridge (Tissot *et al.*, 1996) is therefore reasonable.

2. Materials and methods

2.1. Expression, purification and crystallization of barnase

Wild-type barnase and the three salt-bridge mutants Arg69→Ser (RS69), Asp93→Asn (DN93), Arg69→Ser:Asp93→Asn (RS69:DN93) were expressed and purified as previously described (Tissot *et al.*, 1996). Purified protein was dialysed into water, concentrated to 10–15 mg ml^{-1} and stored in aliquots at 203 K.

All barnase salt-bridge mutants were crystallized under the same conditions as the wild type. Crystals were grown using the hanging-drop method (McPherson, 1982) at 288 or 285 K. A 5 µl drop containing 8–12 mg ml^{-1} protein, 6 m*M* $ZnSO_4$, 0.1 *M* $(NH_4)_2SO_4$ (final concentrations) was suspended over a 1 ml well. The well conditions were 2.58–2.73 *M* ammonium

phosphate pH 7.5, 1–2 m*M* $ZnSO_4$, 0.15–0.30 *M* $(NH_4)_2SO_4$ and 5–10 m*M* NH_4OH. Streak-seeding (Stura & Wilson, 1992) was generally used to induce nucleation, with seeds taken from the wild-type protein. Normally crystals grew within two weeks of set-up; however, crystals of RS69 grew in a drop which was six months old. Initially, crystalline precipitate was observed in this drop. Dissolution of this precipitate by suspending the drop over a well containing 1.89 *M* ammonium phosphate buffer pH 6.1 was followed by re-equilibration of the drop over the original well solution. Streak-seeding of this 're-used' drop induced crystallization for this mutant. Wild-type and mutant crystals grew isomorphously as hexagonal rods of average size 75 × 75 × 250 µm.

2.2. Data processing

Data were collected in-house, using Cu $K\alpha$ radiation from an Elliot GX13 rotating anode, on a MAR Research image plate. The salt-bridge mutant RS69 was the exception; data for this mutant were collected at Daresbury synchrotron. Data sets were indexed and the reflection intensities measured using *MOSFLM* (Collaborative Computational Project, Number 4, 1994). The *CCP*4 suite was used for data reduction (Collaborative Computational Project, Number 4, 1994). 5% of the data set for each mutant was flagged for calculation of the free *R* factor (Brünger, 1992*a*, 1993) during refinement. The same reflections were flagged for all structures to minimize coupling of reflections between calculated and observed structure factors (Kleywegt & Brünger, 1996). Table 2 lists the results of data processing and structure refinement.

2.3. Structure solution, refinement and analysis

The crystals belong to space group $P3_2$, with three molecules per asymmetric unit. Initially, the position of the three molecules within the asymmetric unit was fine-tuned using rigid-body refinement of the wild-type structure. Cycles of maximum-likelihood refinement using *REFMAC* (Murshudov *et al.*, 1997) and model building in *O* (Jones *et al.*, 1991) were used to further improve the model. NCS restraints were used for all structures. During refinement, at least one round of simulated annealing in *X-PLOR* (Brünger, 1992*b*) was included in the early stages and the geometry of the model was checked regularly using *OOPS* (Kleywegt & Jones, 1994*a*) and *PROCHECK* (Collaborative Computational Project, Number 4, 1994). The refinement was considered complete when the free *R* factor could be reduced no further.

Structural comparisons of mutants with the wild type were based on a least-squares fit of C^{α} atoms of the two structures. *LSQMAN* (Kleywegt & Jones, 1994*b*) was used for this purpose. Hydrogen-bond lengths and angles were calculated using *CONTACT* (Collaborative Computational Project, Number 4, 1994).

3. Results

The structure of wild-type barnase is known from both crystallographic and solution studies (Bycroft *et al.*, 1991; Cameron, 1992; Mauguen *et al.*, 1982). Existing crystal structures were solved from data collected at 277 K. Data for the mutants of the Arg69–Asp93 salt bridge were collected from cryocooled crystals at 100 K; therefore, to eliminate differences owing to the temperature of data collection, the structure of the wild-type protein was also determined from data collected at 100 K.

Table 2
Data processing and structure refinement.

Values in parentheses are for the outermost resolution shell.

Protein	Wild-type	RS69	DN93	RS69:DN93
Unit-cell parameters (Å)				
a, *b*	57.63	57.63	57.75	57.78
c	80.98	81.30	81.28	81.42
Resolution (Å)	1.8	1.7	2.0	2.0
R_{merge}†	0.062 (0.187)	0.064 (0.229)	0.069 (0.144)	0.067 (0.144)
Data completeness (%)	96.9 (88.0)	98.1 (86.4)	96.2 (72.2)	91.4 (59.3)
Data multiplicity	1.9 (1.7)	3.5 (3.4)	1.8 (1.5)	1.8 (1.6)
$\langle I/\sigma(I)\rangle$	12.62 (6.50)	13.42 (5.97)	13.73 (5.29)	10.06 (5.10)
Refined model				
R_{cryst}‡ (%	17.3	16.6	17.0	18.8
Free R_{cryst}§ (%)	23.6	21.7	22.8	26.8
Δbond¶ (Å)	0.013	0.012	0.010	0.006
Δangle¶ (°)	1.7	1.4	1.6	1.5
No. of waters††	380	488	354	339
Mean *B*‡‡ (Å^2)	16.89	24.45	17.39	19.29

† R_{merge} is the agreement between multiple measurements of equivalent reflections, defined as $\sum(I_{h,i} - \langle I_h\rangle)/\sum I_{h,i}$, where $I_{h,i}$ are individual intensities and $\langle I_h\rangle$ is the mean value for reflection *h*. ‡ The crystallographic *R* factor is the agreement of the calculated and observed structure factors, defined as $\sum(|F_o - F_c|)/\sum F_o$. § 5% of reflections were omitted from the refinement and used to calculate the free R_{cryst}. Equivalent reflections were taken from each data set. ¶ R.m.s. deviation of bond lengths and angles from ideal geometry for the final model. †† The total number of solvent molecules in the asymmetric unit. ‡‡ The mean isotropic temperature factor for all atoms in the asymmetric unit.

3.1. Interactions of Arg69 and Asp93 in the wild type

Arg69 is situated in $loop_3$ in barnase and Asp93 is in β-$turn_{3-4}$ between the third and fourth β-strands (Fig. 1). $Loop_3$ is the longest loop, spanning 14 residues from Phe56, whose side chain is in the long cleft forming the active site, to Arg69. It is naturally divided into two sub-loops by Leu63, the side chain of which is anchored in hydrophobic $core_3$. The first seven residues of $loop_3$, 56–62, form the guanosine-binding loop; during RNAse activity, a characteristic set of hydrogen bonds to guanosine give barnase G-base specificity (Buckle & Fersht, 1994; Guillet *et al.*, 1993). The remaining residues, 64–69, are referred to here as $loop_{3b}$. The side chain of Arg69 fills the centre of $loop_{3b}$, packing against the main chain of Gly65 and Lys66 (Fig. 2). β-$turn_{3-4}$, a type I β-turn, comprises a hydrogen bond between Ser91 O, the C-terminus of the β_3-strand, and Trp94 N, the N-terminal residue of the β_4-strand.

The salt bridge comprises hydrogen bonds between Arg69 NE and Asp93 OD1, both of which are completely buried from solvent, and between Arg69 NH2 and Asp93 OD2, with a combined solvent-accessible surface area (ASA) of 28.0 Å^2. The side chains of Arg69 and Asp93 are close to the favoured rotamer conformations (Ponder &

Richards, 1987), apart from the torsion angles defining the orientation of the guanidinium group and the carboxylate group: χ_4 and χ_2 are 155 and -17°, respectively, and the guanidinium group and the carboxylate group form a slightly twisted plane. This side-on geometry is typical of an intramolecular arginine–aspartate interaction (Mitchell *et al.*, 1992). The salt-bridge partners make several additional interactions. These hydrogen bonds, as well as other interactions made between $loop_{3b}$ and β-$turn_{3-4}$, are illustrated in Fig. 2.

3.2. Inherent flexibility of $loop_3$ in wild-type barnase

There are three protein chains in the asymmetric unit of wild-type barnase: *A*, *B* and *C*. A least-squares fit of C^α atoms of each chain to every other gives a mean r.m.s. deviation of 0.4 Å. $Loop_{3b}$ has a higher than average deviation (Fig. 3*a*). The electron density for $loop_3$ in the *A* and *B* chains is poor compared with the rest of the chain: in the *A* chain density contoured at 1σ [σ is the r.m.s. deviation in $(2F_o - F_c)$ density] is weak along the backbone of Arg59 and Gly68 and several side chains have no density beyond C^β; in the *B* chain density for these residues is continuous only when contoured at 0.6σ. By contrast, the *C* chain has well defined density for both the main chain and side chains in $loop_3$ (Fig. 3*b*). The mean temperature factor per residue for $loop_3$ in the *A* and *B* chains is significantly higher than the overall mean value (Fig. 3*c*). Once again, the *C* chain is the exception, with temperature factors close to the mean for the chain. A comparison of the crystal contacts made by each chain reveals that $loop_{3b}$ in the *C* chain makes a total of 32 contacts of less than 4.5 Å, with an average contact distance of 3.8 Å; the *A* and *B* chains make 13

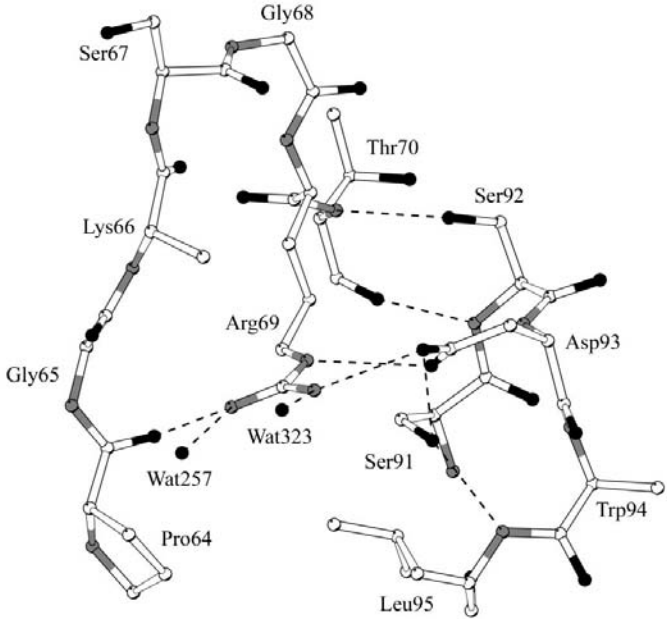

Figure 2
$Loop_{3b}$ and β-$turn_{3-4}$ of wild-type barnase drawn in ball-and-stick representation. Hydrogen bonds formed by the salt bridge and several nearby residues are drawn as dashed lines. All distances were calculated with *CONTACT* (Collaborative Computational Project, Number 4, 1994). Drawn with *BOBSCRIPT* (Esnouf, 1997; Kraulis, 1991).

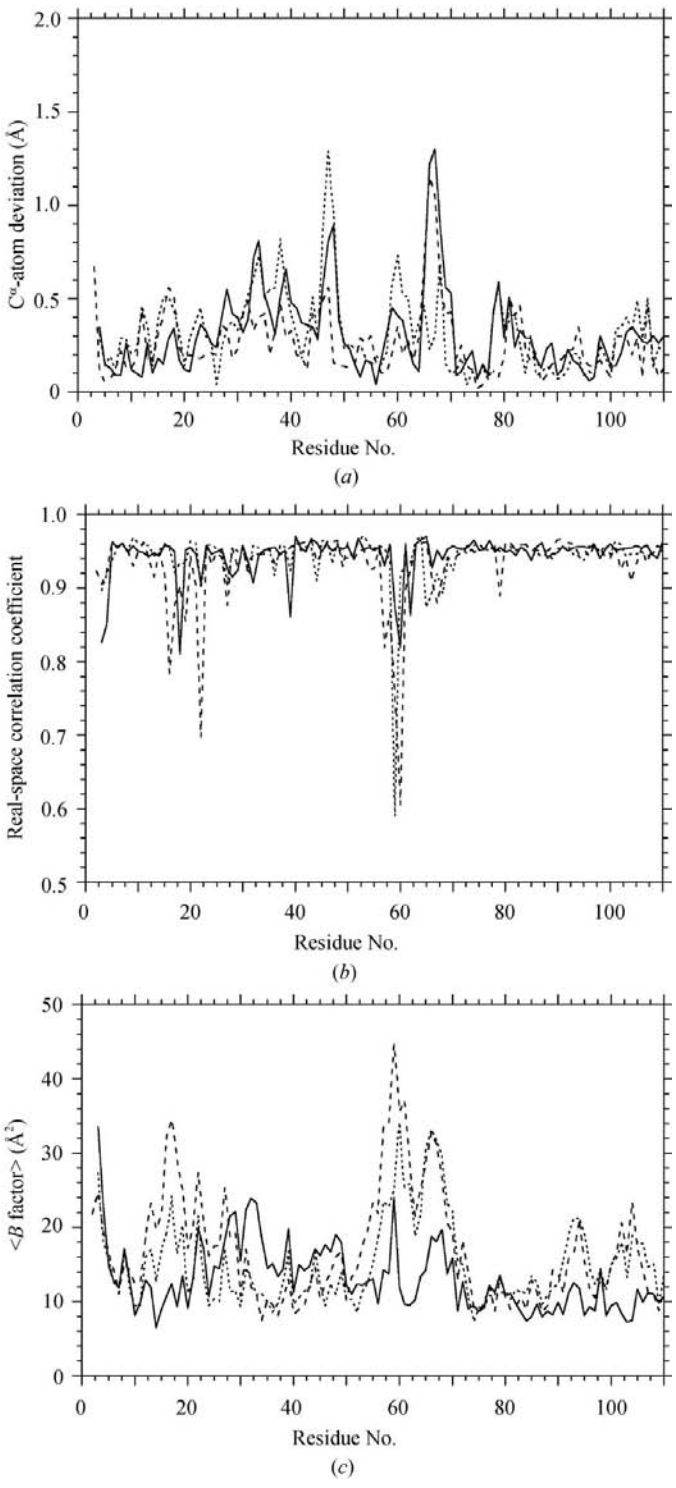

Figure 3
(*a*) Deviation of C^α atoms in a least-squares fit of the three NCS-related chains in the wild-type barnase asymmetric unit. The fit of *A* to *B* is drawn as a broad dashed line, *A* to *C* as a fine dashed line and *B* to *C* as a continuous line. (*b*) Real-space correlation coefficient for the *A* (broad dashed line), *B* (fine dashed line) and *C* chains (continuous line) of wild-type barnase. (*c*) Mean temperature factor per residue for the *A*, *B* and *C* chains of wild-type barnase. The same line types are used as in Fig. 3(*b*).

and 20 such contacts, with mean contact distances of 4.1 and 3.9 Å, respectively. Considering $loop_3$ as a whole (including the GR loop), the *C* chain makes a total of 92 contacts of less than 4.5 Å, compared with only 17 and 28 for the *A* and *B* chains.

Considered together, the least-squares fit of NCS-related molecules, the electron density and the temperature factors suggest that $loop_3$ is inherently flexible. Deviations from the wild-type position of this loop have been observed elsewhere (Baudet & Janin, 1991; Buckle & Fersht, 1994; Guillet *et al.*, 1993). $Loop_{3b}$ in the *C* chain does not exhibit similarly high deviations in temperature factors and electron density because of the restrictions imposed by crystal packing. All structural comparisons are carried out for the *C* chain of barnase.

3.3. Barnase wild-type structures provide a control for the changes observed owing to mutation

A control is needed in order to distinguish differences arising from the inherent flexibility of $loop_{3b}$ from those arising from mutation. This is provided by considering the variation in position of $loop_{3b}$ in several independently solved structures of wild-type barnase. Three wild-type structures at 277 K have been solved from crystals grown at pH 6.0 (PDB code 1bni; Cameron, 1992), pH 7.5 (A. M. Buckle, personal communication) and pH 9.0 (PDB code 1bnj; Cameron, 1992); these are subsequently referred to by the pH at which the crystal was grown. A fourth structure was solved in this study using data collected at 100 K from crystals grown at pH 7.5 (see §2). This is abbreviated to wt herein, since it is the reference wild-type structure for the salt-bridge mutants.

Table 3 lists the results of a least-squares fit of the *C* chains of each wild-type structure to every other. The superposition of structures at pH 6.0 and pH 9.0 has the smallest deviation, closely followed by the fit of the pH 7.5 structure with wt (both at the same pH but with different temperature of data collection). The remaining superpositions, which compare frozen and unfrozen structures or the structure at pH 7.5 with other pH values, all have larger r.m.s. deviations and larger maximum deviations in $loop_{3b}$. In the equivalent fits for the *A* and *B* chains, the maximum deviation of $loop_{3b}$ is considerably larger (the majority are greater than 1 Å; data not shown), further emphasizing the restricted flexibility of $loop_{3b}$ in the *C* chain. In this study, the pH of crystal growth and the temperature of data collection is the same for the wild-type and salt-bridge mutants which have been solved. The inherent deviation of $loop_{3b}$ is therefore unlikely to be greater than that observed for structures at the same pH but different temperature (0.4 Å).

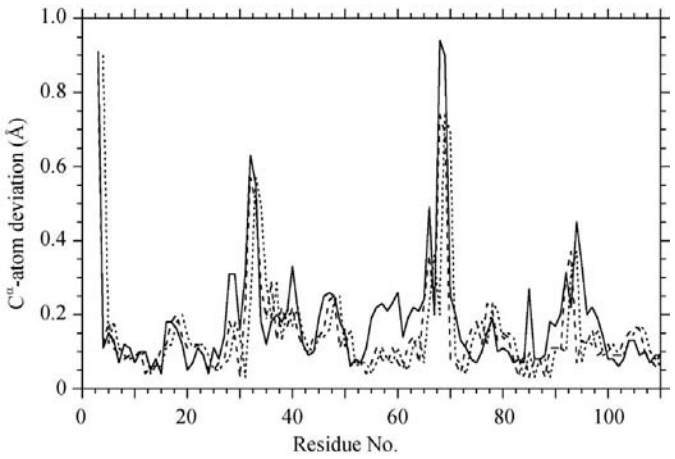

Figure 4
Deviation of C^{α} atoms for the least-squares fit of the *C* chain of each salt-bridge mutant to wild-type barnase. The fit of DN93 is drawn as a fine dashed line, RS69 as a broad dashed line and RS69:DN93 as a continuous line.

Table 3
Deviations of C^{α} atoms in a least-squares fit of four structures of wild-type barnase.

All least-squares fits and r.m.s.d.s were calculated using *LSQMAN* (Kleywegt & Jones, 1994*b*). All C^{α} atoms in the chain were used for these calculations.

			Max. deviation† (Å)	
Superposition‡	Mean r.m.s.d.§ (Å)	R.m.s.d.¶ (Å)	Residues 64–70	Residues 91–95
pH 6.0→pH 9.0	0.3	0.2	0.2 (Arg69)	0.3 (Leu95)
pH 6.0→pH 7.5	0.4	0.4	0.8 (Ser67)	0.5 (Trp94)
pH 6.0→wt	0.4	0.4	0.5 (Gly65)	0.5 (Asp93)
pH 9.0→pH 7.5	0.3	0.3	0.8 (Ser67)	0.4 (Asp93)
pH 9.0→wt	0.4	0.4	0.6 (Lys66)	0.4 (Asp93)
pH 7.5→wt	0.3	0.3	0.4 (Gly65)	0.2 (Asp93)

† The maximum C^{α} deviation in $loop_{3b}$ and β-$turn_{3-4}$ in the fit of the *C* chains, with the residue to which this value belongs in parenthesis. ‡ The four wild-type structures are defined in the main text. § The mean of the r.m.s.d. of C^{α} atoms for each chain within the asymmetric unit. ¶ The r.m.s.d. of C^{α} atoms for the *C* chain only.

Table 4
R.m.s.d. of C^{α} atoms in the least-squares fit of the *C* chain of each mutant to wild type.

	R.m.s.d.† (Å)			Max.
Superposition	Overall	Residues 64–70	Residues 91–95	deviation‡ (Å)
DN93→WT	0.2 (1.9)	0.5 (1.4)	0.3 (2.8)	0.9
RS69→WT	0.2 (5.0)	0.4 (10.4)	0.2 (5.31)	0.7
RS69:DN93→WT	0.2 (3.7)	0.6 (5.3)	0.3 (3.5)	0.9

† The r.m.s. difference in the position of C^{α} atoms. The r.m.s. difference in temperature factor ($Å^2$) of C^{α} atoms is listed in parentheses. ‡ The maximum difference in C^{α} position in the least-squares fit. This occurs for Gly68 in all mutants.

3.4. DN93

The deviation of C^{α} atoms for each residue in the fit of wild type and DN93 is shown in Fig. 4. The r.m.s. deviation is 0.2 Å for C^{α} atoms; for residues 64–70 and 91–95 only, this value is 0.5 and 0.3 Å, respectively (Table 4). The deviation observed for all C^{α} atoms is low compared with those amongst different wild-type structures. Overall, this mutant resembles the wild type. There is an outward shift of Ser67–Arg69 to a maximum of 0.9 Å away from the side chain of Asn93 (Fig. 5*a*). Despite this backbone movement, the side chain of Arg69, in particular the guanidinium group, remains in approximately the same position as in the wild type. In β-$turn_{3-4}$, there is a backbone shift of up to 0.5 Å for Asn93 and Trp94 away from

loop$_{3b}$. This conservative mutation does not create a cavity, as predicted (Tissot *et al.*, 1996).

The amide group of the mutated Asn93 changes orientation relative to the wild type. χ_2 changes to 137°; steric hindrance from Ser91 OG prevents a more favourable angle being occupied. This new χ angle increases the solvent accessibility of this side chain to 55 Å^2, compared with 46 Å^2 in the wild type. The relative orientation of the OD1 and ND2 atoms of the amide group of Asn93 in this mutant is unclear from the electron density and the temperature factors. It seems likely, however, that the shortest interaction between the guanidinium group and the amide group is between atoms of opposite polarity. In this case, Asn93 OD1 is solvent accessible and forms a charge–polar hydrogen bond with Arg69 NH2; Asn93 ND2 is inaccessible to solvent, pointing towards the centre of the loop (Fig. 6*a*). In this orientation, the single-mutant atoms Asn93 OD1 and Asn93 ND2 are structurally equivalent to wild-type Asp93 OD2 and Asp93 OD1, respectively. The separation of the interacting arginine and Asn93 has increased by more than 0.5 Å relative to the wild type. Although the separation of Asn93 OD1 and Arg69 NH2 is the shortest distance between the two residues, it is still relatively long for a strong hydrogen bond. Asn93 ND2 makes a single hydrogen bond with the only new water molecule, Wat147, observed in this mutant (Fig. 6*a*). No new hydrogen bonds between loop$_{3b}$ and β-turn$_{3-4}$ are formed and all other interactions made in the wild type are made in this single mutant.

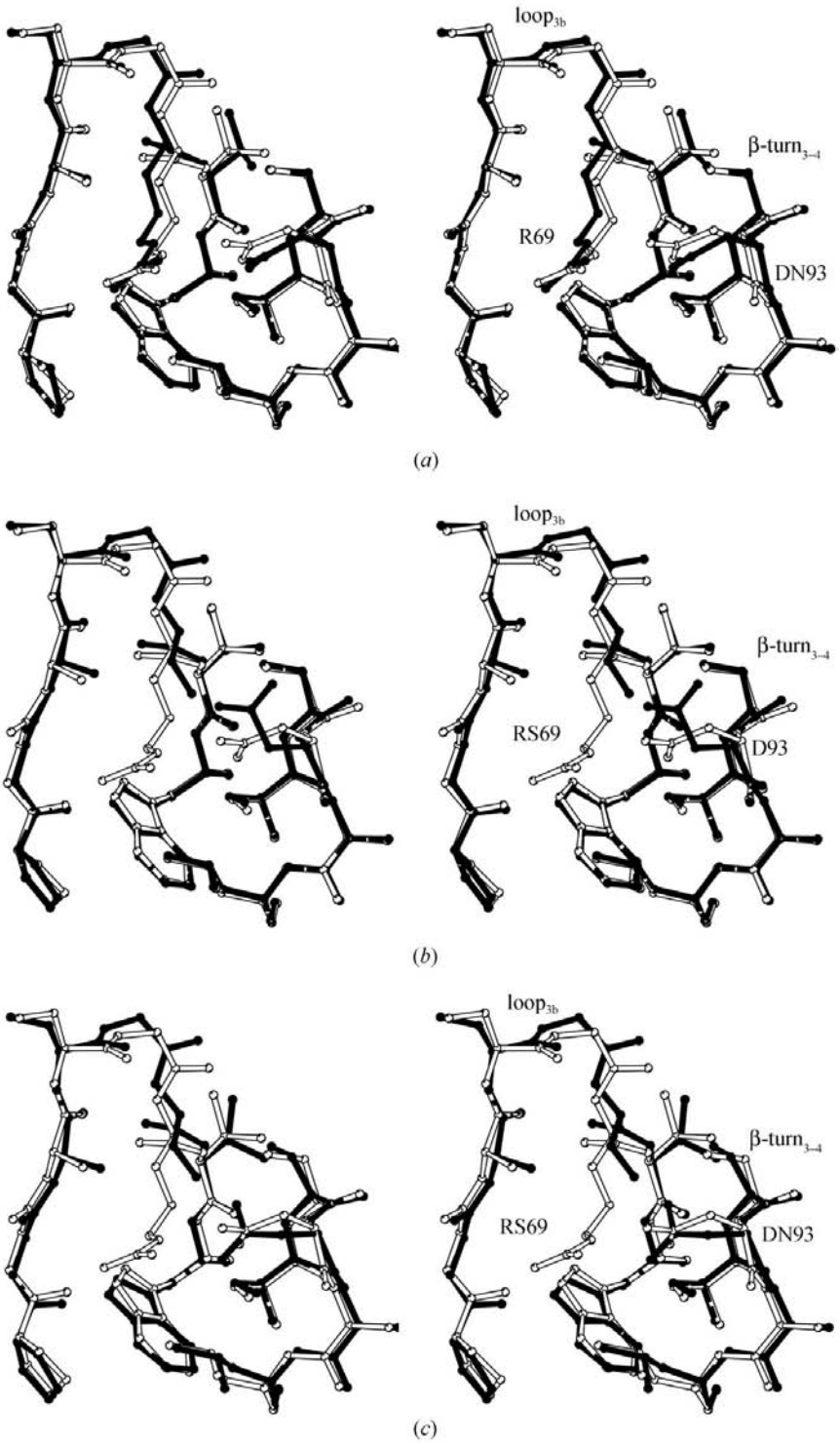

Figure 5
A stereoview of the least-squares superposition of each mutant with the wild type. In each view loop$_{3b}$ is on the left and β-turn$_{3-4}$ is on the right of the image. (*a*) DN93, (*b*) RS69, with only the *A* rotamer of Arg69→Ser drawn for clarity, (*c*) RS69:DN93. The wild type is drawn in white and the mutant in black. Drawn with *BOBSCRIPT* (Esnouf, 1997; Kraulis, 1991).

There is no significant increase in the mean temperature factors per residue of loop$_{3b}$ relative to the mean value for the whole chain and in this respect DN93 also resembles the wild-type protein. This suggests that the salt bridge alone is not responsible for maintaining the mean temperature factors of this loop.

As well as the changes in main-chain position around the site of mutation, residues 32–33 at the C-terminus of the α_2 helix show shifts greater than 0.5 Å in the fit of this mutant to the wild type (Fig. 4). These changes are a result of crystal packing, however, since they make contacts with loop$_{3b}$ and are observed in all three mutants of the double-mutant cycle.

3.5. RS69

The deviation of C$^\alpha$ atoms for each residue in the fit of wild type and the single mutant RS69 is shown in Fig. 4. The r.m.s. deviation for C$^\alpha$ atoms is 0.2 Å; the r.m.s. deviation for C$^\alpha$ atoms in loop$_{3b}$ only is

0.4 Å and that for residues 91–95 is 0.2 Å (Table 4). The overall deviation of C^{α} atoms is the same for DN93; however, DN93 has larger deviations in $loop_{3b}$ and β-$turn_{3-4}$.

Residues Gly65 and Lys66 collapse to a small extent into the cavity created by the mutation of the Arg69 side chain (Fig. 5*b*). Ser67–Ser69 shifts in the opposite direction, away from the wild-type position and the rest of the protein, by a maximum of 0.7 Å. The main chain from Ser91 to Leu95 changes little compared with the wild type. All side chains in $loop_{3b}$ and β-$turn_{3-4}$ remain in the same conformation as in the wild type, except for the salt-bridge partners Ser69 and Asp93. The electron density clearly defines two possible conformations for the side chain of Ser69. The *A* rotamer maintains approximately the same χ_1 angle as the wild-type Arg69; this is close to one of the preferred rotamers of the serine side chain (Ponder & Richards, 1987). In this rotamer the hydroxyl group lies in the plane of the loop, whereas in the *B* rotamer the side chain points out of the loop. On deletion of the guanidinium group of Arg69, the side chain of Asp93 changes conformation (χ_1 and χ_2 are −59 and 121°, respectively; Fig. 5*a*).

In its new conformation, Asp93 OD1 forms a hydrogen bond with each rotamer of the mutated disordered Ser69 OG, which together count as a whole. The direct hydrogen bond with Ser91 OG made in the wild type is lost and is replaced by a water-mediated hydrogen bond in this mutant. In addition to the new interaction with the carboxylate group of Asp93, each rotamer of the Ser69 side chain makes a new hydrogen bond with Ser92 OG, which together can be considered as a whole.

Four new water molecules enter the cavity created at the centre of the loop by the mutation of the arginine group and the change in the conformation of the aspartate side chain. These are Wat78, Wat429, Wat454 and Wat254. Wat78 and Wat429 occupy the space equivalent to the arginine side chain in the wild type. Wat454 sits in front and Wat254 behind this. A

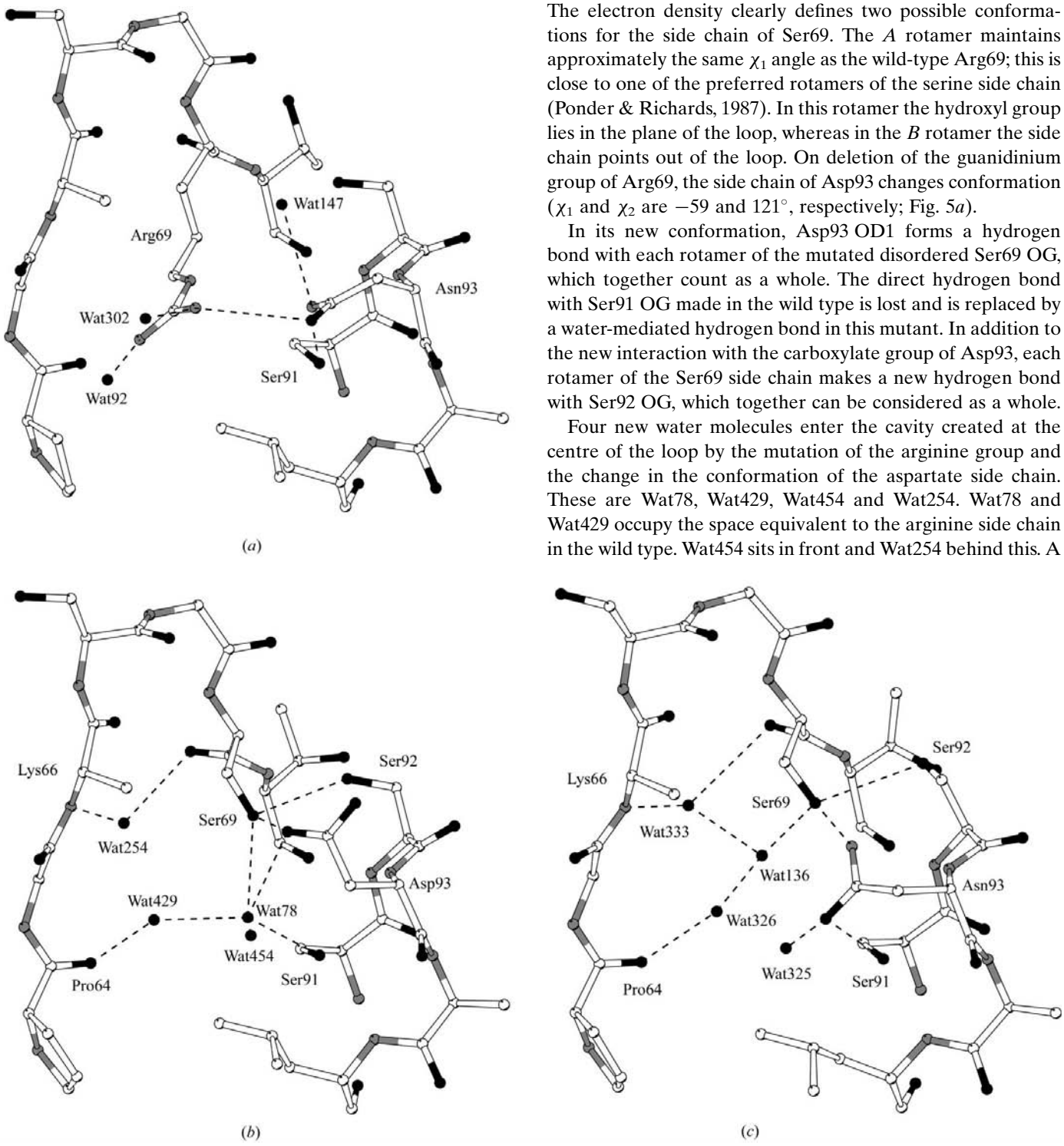

Figure 6
$Loop_{3b}$ and β-$turn_{3-4}$ of each mutant structure drawn in ball-and-stick representation, including new water molecules which enter the site of mutation or form hydrogen bonds with the mutated residues. New hydrogen bonds are drawn as dashed lines. (*a*) DN93, (*b*) RS69, with only the *A* rotamer of the Arg69→Ser side chain drawn for clarity, (*c*) RS69:DN93. All distances were measured using *CONTACT* (Collaborative Computational Project, Number 4, 1994). Drawn with *BOBSCRIPT* (Esnouf, 1997; Kraulis, 1991).

network of hydrogen bonds are made by these water molecules (Fig. 6*b*).

The remaining interactions made by $loop_{3b}$ and β-$turn_{3-4}$ in the wild type are made in this single mutant. Two waters which hydrogen bond to the guanidinium group of Arg69 in the wild type have no equivalent in this mutant. These are Wat257 and Wat323, which form hydrogen bonds with Arg69 NH1 and NH2, respectively (the latter is long for a hydrogen bond).

Temperature factors for $loop_{3b}$ in RS69 increase significantly relative to the mean overall temperature factor for the *C* chain. This suggests that the interactions made by Arg69 in the wild type are important for reducing the flexibility of $loop_{3b}$.

3.6. RS69:DN93

The fit of the *C* chain of this double mutant to the wild type has an r.m.s. deviation of C^{α} atoms of 0.2 Å (Table 4). For residues 64–70 and 91–95, the r.m.s. deviation is 0.6 and 0.3 Å, respectively, which is a higher deviation than for either of the single mutants. There is a collapse of the backbone at Lys66 of up to 0.49 Å into the site of the Ser69 mutation. By contrast, Gly68 and Ser69 shift away from the wild-type position by up to 0.9 Å. Around the site of the Asn93 mutation no shift is observed for the main chain of residues 91–93; however, the backbone of Trp94 and Leu95 moves away from $loop_{3b}$ by a maximum of 0.5 Å.

The side chain of Ser69 in the double mutant has approximately the same χ_1 angle as the wild-type arginine; the side chain therefore lies in the plane of the loop (Fig. 5*c*). The mutated side chain of Asn93 stays in roughly the same position as in the wild type; however, the side-chain dihedral angles become unfavourable (χ_1 and χ_2 of 16 and 120°, respectively). The strained conformation allows both OD1 and ND2 of Asn93 to form hydrogen bonds.

Asn93 ND2 points into $loop_{3b}$, where it forms one hydrogen bond with Ser69 OG (Fig. 6*c*). This interaction is equivalent to that made between Ser69 OG and Asp93 OD1 in the single mutant RS69. Asn93 OD1 maintains the interaction with Ser91 OG found in the wild type. In addition to its interaction with Asn93, Ser69 OG forms a hydrogen bond with Ser92 OG. This hydrogen bond is also made in the single mutant RS69.

Four new water molecules, Wat136, Wat325, Wat326 and Wat333, enter the created cavity, with Wat136 and Wat326 occupying the space of the truncated arginine and Wat325 and Wat333 in front of and behind this, repectively. They form a network of hydrogen bonds within the created cavity (Fig. 6*c*). Three of the four new waters observed have a direct equivalent in the single mutant RS69: Wat325 is equivalent to Wat454 in the single mutant, and Wat326 and Wat333 to Wat429 and Wat254, respectively. The wild-type water molecule Wat323, which hydrogen bonds to Arg69 NH2, has no equivalent in this double mutant. It is also missing from the single mutant RS69.

The average temperature factor per residue increases dramatically for $loop_{3b}$ in the double mutant relative to the mean of all residues. This distribution of temperature factors resembles the single mutant RS69. The loop is therefore considerably more flexible than in the wild type.

3.7. Structural rationalization of stability changes

All mutations in this double-mutant cycle result in only minor local rearrangement despite each mutant being considerably destabilized relative to the wild type (Table 1). The mutant with greatest destabilization, DN93, most resembles the wild type in structure. In DN93, two of the three amino groups in the unpaired side chain of Arg69, NH1 and NH2, make charge–polar hydrogen bonds. A possible explanation for the large destabilization of this mutant is that the third amino group, NE, which is buried within $loop_{3b}$, makes no interactions. The importance of fulfilling hydrogen-bonding potential has been noted previously in T4 lyosyme (Alber *et al.*, 1987). These results contrast with the structural consequences of disrupting a buried arginine–asparate salt bridge in chloramphenicol acetyl transferase (Gibbs *et al.*, 1990). In this protein, mutating the asparate to asparagine results in both partners of the salt-bridge changing conformation entirely, as well as other local side-chain rearrangements and backbone movements up to 20 Å from the site of mutation; all polar and charged groups of the mutated salt bridge form hydrogen bonds in their new orientations. Interestingly, this mutant has the same stability as the wild-type protein.

The least destabilized salt-bridge mutant RS69 replaces arginine, a hydrogen-bond donor, with serine, which can both donate and accept hydrogen bonds. In the single mutant, the hydroxyl group of the mutant Ser69 donates a hydrogen bond to the remaining salt-bridge partner Asp93 and accepts a hydrogen bond from the hydroxyl group of Ser92 in β-$turn_{3-4}$. The structures of this mutant and the double mutant resemble one another, but the double mutant is 3.2 kJ mol^{-1} less stable. In RS69:DN93, Ser69 forms an equivalent hydrogen bond with residue 93, although in this case the hydroxyl group accepts a H atom from Asn ND2. This hydrogen bond is a polar–polar interaction compared with the charge–polar interaction of the single mutant RS69. Deleting a charged hydrogen-bonding group at an enzyme–substrate interface decreases the binding energy by more than twice that of a polar–polar interaction (Fersht *et al.*, 1985). This may be the primary source of the destabilization of the double mutant relative to RS69. In addition, the side chain of Asn93 in the double mutant has considerably fewer favourable torsion angles than its equivalent in RS69 and, unlike RS69, there is no water-mediated interaction between Asp93 and Pro64. In both RS69 and the double mutant the cavity created by the truncation of the arginine side chain is filled by four water molecules. A similar mutation at a dimer–dimer interface of gene V protein (GVP) from Ff phage, Arg82→Cys, results in the collapse of a neighbouring side chain into the site of mutation; no water is observed in the created cavity (Su *et al.*, 1997).

It has been suggested that the Arg69–Asp93 salt bridge contributes to the folding of barnase by limiting the number of conformations available (Oliveberg & Fersht, 1996; Tissot *et al.*, 1996), since buried but unpaired charges are highly

destabilizing. Consequently, Arg69 has been proposed as an example of a 'structural' arginine (Borders *et al.*, 1994; Mrabet *et al.*, 1992; Tissot *et al.*, 1996). Examining the temperature factors for $loop_{3b}$ in the wild type and each of the mutants clearly illustrates that it is primarily the arginine side chain and not the salt bridge which is responsible for maintaining native-like flexibility of this loop, thus further supporting the original observation (Tissot *et al.*, 1996).

3.8. The double-mutant cycle in relation to the single- and double-mutant structures

For the interaction between *X* and *Y* in a protein *E-XY*, a thermodynamic cycle is contructed consisting of the wild type, *E-XY*, two single mutants in which *X* and *Y* are mutated to *A* and *B*, respectively, and the double mutant in which both *X* and *Y* are simultaneously mutated to *A* and *B*. The difference between parallel sides of this cycle is the interaction energy, $\Delta\Delta G_{\rm int}$,

$$\begin{aligned}\Delta\Delta G_{\rm int} &= \Delta\Delta G_{E\text{-}XY\rightarrow E\text{-}XB} + \Delta\Delta G_{E\text{-}AY\rightarrow E\text{-}AB} \\ &= \Delta\Delta G_{E\text{-}XY\rightarrow E\text{-}AY} + \Delta\Delta G_{E\text{-}XB\rightarrow E\text{-}AB}. \qquad (2)\end{aligned}$$

Ideally, there are no changes in structure on mutation of *E* or any structural changes in the single mutant are also present in the double mutant and the energy associated with these changes will cancel in the cycle. $\Delta\Delta G_{\rm int}$ then reduces to the interaction energy plus the change in solvation of *X* and *Y* on mutating their partner (Fersht *et al.*, 1992; Serrano *et al.*, 1990).

From an analysis of each structure within the cycle constructed for the Arg69–Asp93 salt bridge, it is clear that all direct hydrogen bonds formed between residues in $loop_{3b}$ and β-$turn_{3-4}$ cancel. The exception is the interaction between Asp93 and Ser91. The direct hydrogen bond made between these residues in the wild type is lost in the single mutant DN93; however, it is replaced by a water-mediated interaction, so it is compensated for to some extent.

Changes in solvation parallel the changes in structure in that DN93 resembles the wild type and RS69 resembles the double mutant. The formation of a new hydrogen bond with a water molecule at the surface of a protein is an isoenthalpic process (Fersht *et al.*, 1985), since in bulk solvent the water will hydrogen bond with another water. There is, however, an entropy cost in localizing the water molecule at the protein surface. This has been estimated to be worth $\leq$8.4 kJ mol^{-1} per water (Dunitz, 1994). Considering only water molecules which make hydrogen bonds with the salt-bridge residues and those which enter the site of mutation, a net of zero water molecules are localized within the cycle.

Analysis of the structural changes in this double-mutant cycle therefore reduces to the set of interactions formed between residues 69 and 93 in each structure. In the single mutant RS69 and the double mutant RS69:DN93 there is one hydrogen bond, between the hydroxyl group of Ser69 and side chain of Asp93 and Asn93, respectively. These interactions therefore cancel, leaving the Arg69–Asp93 interaction in the wild type and the Arg69–Asn93 interaction in the single mutant DN93. In the wild type this comprises two hydrogen bonds plus the electrostatic component. In DN93 this is a single charge–polar hydrogen bond. Consequently, the measured interaction energy of -14.0 ± 0.62 kJ mol^{-1} (Table 1) is the sum of the electrostatic component of the Arg69–Asp93 interaction plus a single hydrogen bond.

The strength of a hydrogen bond varies widely depending upon the context of the interaction. Deletion of largely buried hydrogen bonds in barnase and T4 lysosyme destabilize the protein by $\sim$2.1–8.4 kJ mol^{-1} (Alber *et al.*, 1987; Chen *et al.*, 1993; Serrano *et al.*, 1992). Deletion of uncharged hydrogen-bonding groups involved in substrate binding reduces the binding free energy to tyrosyl-tRNA synthetase by 2.1–6.3 kJ mol^{-1}, whereas deletion of a charged group reduces the binding free energy by 12.5–18.8 kJ mol^{-1} (Fersht *et al.*, 1985). It is difficult, therefore, to estimate precisely the strength of the electrostatic interaction; however, it could potentially have a maximum value near 12.5 kJ mol^{-1}.

Elsewhere, the contribution of buried salt bridges to protein stability has been estimated by measuring the change in pK_a on titration of a one partner in the salt bridge (Anderson *et al.*, 1990; Fersht, 1972), by desolvation experiments on *de novo* designed peptides (Wimley *et al.*, 1996) and by substitution of the charged residues by hydrophobic residues (Hendsch & Tidor, 1994; Waldburger *et al.*, 1995). Interaction energies measured from the double-mutant cycle are fundamentally different from the energies estimated from these methods. The double-mutant cycle analysis (Carter *et al.*, 1984; Horovitz, 1987; Horovitz & Fersht, 1990; Serrano *et al.*, 1990) of the electrostatic interaction between residues in a salt bridge gives an estimate of their true interaction energy in the ideal situation where there is no structural rearrangement on mutation to the single and double mutants in the cycle (Fersht *et al.*, 1992; Serrano *et al.*, 1990). It is a measure of the strength of the electrostatic interaction in the folded relative to the unfolded state, where in a random coil conformation they are presumed to interact only with solvent and not with each other.

Since double-mutant cycles were first used to measure the cooperative effects of residues within the active site of tyrosyl tRNA synthetase on binding of ATP (Carter *et al.*, 1984), the method has been incorporated as an additional tool within the field of protein engineering (Horovitz & Fersht, 1990; Wells, 1990), measuring the strength of specific interactions between proteins (Ackermann *et al.*, 1998; Goldman *et al.*, 1997; Schreiber & Fersht, 1995), within proteins (de Vos *et al.*, 1992; Horovitz *et al.*, 1990; Jackson & Fersht, 1994; Licata & Ackers, 1995; Loewenthal *et al.*, 1992; Marqusee & Sauer, 1994; Sali *et al.*, 1991; Serrano *et al.*, 1990, 1991) and designed helical peptides (Krylov *et al.*, 1994; Zhou *et al.*, 1994*a*) and during the folding process (Horovitz, 1992; Horovitz *et al.*, 1991; Itzhaki *et al.*, 1995). In many of these examples the energetic analysis is accompanied by structural studies, notably using NMR techniques, confirming that the mutations do not lead to significant structural changes. This study underlines the importance of structural information in interpreting interaction energies measured using this method and highlights the robust nature of the double-mutant cycle analysis.

References

Ackermann, E. T., Ang, H., Kanter, J. R., Tsigelny, I. & Taylor, P. (1998). *J. Biol. Chem.* **273**, 10958–10964.
Alber, T., Dao-Pin, S., Wilson, K., Wozniak, J. A., Cook, S. P. & Matthews, B. M. (1987). *Nature (London)*, **330**, 41–46.
Anderson, D. E., Becktel, W. J. & Dahlquist, F. W. (1990). *Biochemistry*, **29**, 2403–2408.
Baudet, S. & Janin, J. (1991). *J. Mol. Biol.* **219**, 123–132.
Borders, C. L. J., Broadwater, J. A., Bekeny, P. A., Salmon, J. E., Lee, A. S., Eldridge, A. M. & Pett, V. B. (1994). *Protein Sci.* **3**, 541–548.
Brünger, A. T. (1992*a*). *Nature (London)*, **355**, 472–475.
Brünger, A. T. (1992*b*). *X-PLOR Manual, Version* 3.0. Yale University, New Haven, Connecticut, USA.
Brünger, A. T. (1993). *Acta Cryst.* D**49**, 24–36.
Buckle, A. M. & Fersht, A. R. (1994). *Biochemistry*, **33**, 1644–1653.
Bycroft, M., Ludvingen, S., Fersht, A. R. & Poulsen, F. M. (1991). *Biochemistry*, **30**, 8697–8701.
Cameron, A. D. (1992). PhD thesis. University of York, England.
Carter, P. J., Winter, G., Wilkinson, A. J. & Fersht, A. R. (1984). *Cell*, **38**, 835–840.
Cavagnero, S., Debe, D. A., Zhou, Z. H., Adams, M. W. W. & Chan, S. I. (1998). *Biochemistry*, **37**, 3369–3376.
Chen, Y. W., Fersht, A. R. & Henrick, K. (1993). *J. Mol. Biol.* **234**, 1158–1170.
Collaborative Computational Project, Number 4 (1994). *Acta Cryst.* D**50**, 760–763.
Dao-Pin, S., Sauer, U., Nicholson, H. & Matthews, B. W. (1991). *Biochemistry*, **30**, 7142–7153.
Dunitz, J. D. (1994). *Science*, **264**, 670.
Esnouf, R. M. (1997). *J. Mol. Graph.* **15**, 132.
Fersht, A. R. (1972). *J. Mol. Biol.* **64**, 497–509.
Fersht, A. R., Matouschek, A. & Serrano, L. (1992). *J. Mol. Biol.* **224**, 771–782.
Fersht, A. R., Shi, J.-P., Knill-Jones, J., Lowe, D. M., Wilkinson, A. J., Blow, D. M., Brick, P., Carter, P., Waye, M. M. Y. & Winter, G. (1985). *Nature (London)*, **314**, 235–238.
Gibbs, M. R., Moody, P. C. E. & Leslie, A. G. W. (1990). *Biochemistry*, **29**, 11261–11265.
Goldman, E. R., DallAcqua, W., Braden, B. C. & Mariuzza, R. A. (1997). *Biochemistry*, **36**, 49–56.
Guillet, V., Lapthorn, A. & Mauguen, Y. (1993). *FEBS Lett.* **330**, 137–140.
Hendsch, Z. S. & Tidor, B. (1994). *Protein Sci.* **3**, 211–226.
Horovitz, A. (1987). *J. Mol. Biol.* **196**, 733–735.
Horovitz, A. (1992). *J. Mol. Biol.* **224**, 733–740.
Horovitz, A. & Fersht, A. R. (1990). *J. Mol. Biol.* **214**, 613–617.
Horovitz, A., Serrano, L., Avron, B., Bycroft, M. & Fersht, A. R. (1990). *J. Mol. Biol.* **216**, 1031–1044.
Horovitz, A., Serrano, L. & Fersht, A. R. (1991). *J. Mol. Biol.* **219**, 5–9.
Itzhaki, L. S., Otzen, D. E. & Fersht, A. R. (1995). *J. Mol. Biol.* **254**, 260–288.
Jackson, S. E. & Fersht, A. R. (1994). *Biochemistry*, **33**, 13880–13887.
Jones, T. A., Zou, J. Y., Cowan, S. W. & Kjeldgaard, M. (1991). *Acta Cryst.* A**47**, 110–119.
Kleywegt, G. J. & Brünger, A. T. (1996). *Structure*, **4**, 897–904.
Kleywegt, G. J. & Jones, T. A. (1994*a*). *Jnt CCP4/ESF–EACBM Newsl. Protein Crystallogr.* **30**, 20–24.
Kleywegt, G. J. & Jones, T. A. (1994*b*). *Jnt CCP4/ESF–EACBM Newsl. Protein Crystallogr.* **31**, 9–14.
Kraulis, P. (1991). *J. Appl. Cryst.* **24**, 946–950.
Krylov, D., Mikhailenko, I. & Vinson, C. (1994). *EMBO J.* **13**, 2849–2861.
Licata, V. J. & Ackers, G. K. (1995). *Biochemistry*, **34**, 3133–3139.
Loewenthal, R., Sancho, J. & Fersht, A. R. (1992). *J. Mol. Biol.* **224**, 759–770.
McPherson, A. (1982). *The Preparation and Analysis of Protein Crystals.* New York: John Wiley & Sons.
Marqusee, S. & Sauer, R. T. (1994). *Protein Sci.* **3**, 2217–2225.
Mauguen, Y., Hartley, R. W., Dodson, E. J., Dodson, G. G., Bricogne, G., Chothia, C. & Jack, A. (1982). *Nature (London)*, **29**, 162–164.
Merritt, E. A. & Bacon, D. J. (1997). *Methods Enzymol.* **277**, 505–524.
Mitchell, J. B. O., Thornton, J. M. & Singh, J. (1992). *J. Mol. Biol.* **226**, 251–262.
Monera, O. D., Kay, C. M. & Hodges, R. S. (1994). *Biochemistry*, **33**, 3862–3871.
Mrabet, N. T., Van den Broeck, A., Van den Brande, I., Stanssens, P., Laroche, Y., Lambeir, A., Matthijssens, G., Jenkins, J., Chiadmi, M., van Tilbeurgh, H., Rey, F., Janin, J., Quax, W. J., Lasters, I., De Maeyer, M. & Wodak, S. (1992). *Biochemistry*, **31**, 2239–2253.
Murshudov, G. N., Vagin, A. A. & Dodson, E. J. (1997). *Acta Cryst.* D**53**, 240–255.
Oliveberg, M. & Fersht, A. R. (1996). *Biochemistry*, **35**, 6795–6805.
O'Shea, E. K., Rutkowski, R. & Kim, P. S. (1992). *Cell*, **68**, 699–708.
Ponder, J. & Richards, F. (1987). *J. Mol. Biol.* **193**, 775–791.
Prat Gay, G. de, Johnson, C. M. & Fersht, A. R. (1994). *Protein Eng.* **7**, 103–108.
Sali, D., Bycroft, M. & Fersht, A. R. (1991). *J. Mol. Biol.* **220**, 779–788.
Schneider, J. P., Lear, J. D. & DeGrado, W. F. (1997). *J. Am. Chem. Soc.* **119**, 5742–5743.
Schreiber, G. & Fersht, A. R. (1995). *J. Mol. Biol.* **248**, 478–486.
Serrano, L., Bycroft, M. & Fersht, A. R. (1991). *J. Mol. Biol.* **218**, 465–475.
Serrano, L., Horovitz, A., Avron, B., Bycroft, M. & Fersht, A. R. (1990). *Biochemistry*, **29**, 9343–9352.
Serrano, L., Matouschek, A. & Fersht, A. R. (1992). *J. Mol. Biol.* **224**, 805–818.
Stura, E. A. & Wilson, I. A. (1992). In *Crystallization of Nucleic Acids and Proteins. A Practical Approach*, edited by A. Ducruix & R. Giegé. Oxford University Press.
Su, S., Gao, Y., Zhang, H., Terwilliger, T. C. & Wang, A. H. J. (1997). *Protein Sci.* **6**, 771–780.
Tissot, A. C., Vuilleumier, S. & Fersht, A. R. (1996). *Biochemistry*, **35**, 6786–6794.
Vinson, C. R., Hai, T. & Boyd, S. M. (1993). *Genes Dev.* **7**, 1047–1058.
Vos, A. M. de, Ultsch, M. & Kossiakoff, A. A. (1992). *Science*, **255**, 306–313.
Waldburger, C. D., Jonsson, T. & Sauer, R. T. (1996). *Proc. Natl Acad. Sci. USA*, **93**, 2629–2634.
Waldburger, C. D., Schildbach, J. F. & Sauer, R. T. (1995). *Nature Struct. Biol.* **2**, 122–128.
Wells, J. A. (1990). *Biochemistry*, **29**, 8509–8517.
Wimley, W. C., Gawrisch, K., Creamer, T. P. & White, S. H. (1996). *Proc. Natl Acad. Sci. USA*, **93**, 2985–2990.
Zhou, N. E., Kay, C. M. & Hodges, R. S. (1994*a*). *Protein Eng.* **7**, 1365–1372.
Zhou, N. E., Kay, C. M. & Hodges, R. S. (1994*b*). *J. Mol. Biol.* **237**, 500–512.